SLAC-56
UC-28, Particle Accelerators
and High-Voltage Machines
TID-4500 (48th Ed.)

A COMPUTER CODE FOR VARIABLE PERMEABILITY MAGNETOSTATIC FIELD PROBLEMS

by

E. A. Burfine, L. R. Anderson, H. Brechna

April 1966

Technical Report
Prepared Under
Contract AT(04-3)-515
for the USAEC
San Francisco Operations Office

Printed in USA. Price $3.00. Available from the Clearinghouse for Federal Scientific and Technical Information (CFSTI), National Bureau of Standards, U. S. Department of Commerce, Springfield, Virginia.

TABLE OF CONTENTS

LIST OF FIGURES

LIST OF SYMBOLS

A	Magnetic Vector Potential
A_θ	θ Component of the Magnetic Vector Potential
A_z	z Component of the Magnetic Vector Potential
A_E	Notation for Location of A in the Mesh
A_N	
A_{NN}	
A_O	
A_S	
A_W	
B	Flux Density
C	Curve
C_m	Scaling Factor for the mth Line Integral
D	Displacement
G_μ	Relative Permeability as a Function Field Intensity
g	Variational Function
H	Field Intensity
h	Mesh Size
I	Current
$\hat{i}, \hat{j}, \hat{k}$	Unit Vectors
ℓ	Path Length
N	Number of Turns
p, q	Number of Nodes
R	Residual
R_n	Residual after nth Iteration

r	Radius
S	Current Density
s	Area
t	Time
x, y, z	Cartesian Coordinates
δ_n	Relative Error after n Iterations
δ_I, δ_{II}	Relative Errors in Phase I and II
$\hat{\epsilon}_1, \hat{\epsilon}_2, \hat{\epsilon}_3$	Base Vectors in Cylindrical Coordinates
ϵ	Mathematical Symbol for the Member of a Set
θ	Angle
λ	Space or Fill Factor
μ	Permeability
μ_r	Relative Permeability
μ_o	Permeability of Vacuum
μ_E, μ_N, μ_O, μ_S, μ_W	Notation for the Location of Permeabilities
ρ	Radius of a Circle, Which Contains the Field Region
ω	Relaxation Coefficient for Magnetic Vector Potential
ω_μ	Relaxation Coefficient for Permeability

ABSTRACT

A method for solving variable permeability two-dimensional and axially symmetric magnetostatic problems will be discussed and the implementation of this method in the computer code NUTCRACKER explained.

I. INTRODUCTION

The computer code NUTCRACKER has been used in the design studies of iron bound and iron core magnets with complicated geometries, such as C and H type beam transport magnets, spark chamber magnets, and bubble chamber magnets. The program is able to solve the following problems:

(a) Vector potential in and outside the iron body.

(b) Distribution of relative permeability in a two-dimensional area.

(c) Quasi-linear partial differential equations arising in two-dimensional magnetostatic field problems.

(d) Field distribution in and outside the iron body.

In general, any problem to which the following assumptions may be applied can be solved by the computer program:

(a) Zero or constant vector potential on the boundary, which can be chosen arbitrarily.

(b) Rectangular region of interest.

(c) Square mesh in finite difference equation.

(d) Either axial symmetry or doubly infinite symmetry.

For many applications the above assumptions are not restrictive. However, in case of curved boundaries the present code needs further improvement.

A. Problem Formulation

At present several computer codes for solving magnetostatic problems are in operation.[1,2,4,5,6,12,13] These codes fall into two categories:

(a) Iron permeability is assumed to be constant over the entire iron.[1,2] This assumption leads to the solution of the Poisson equation:

$$\nabla^2 A = -\mu S \quad . \tag{1}$$

This calculation leads to errors in the computation of the magnetic fields in excess of 10% and if the iron is nearly saturated the effect of these errors may prove to be disturbing. However, the code is efficient and the approximation is quite useful if $\mu_r >> 1$.

(b) Iron permeability is variable throughout the magnet return path. The deficiency of category (a) for highly saturated ferromagnetic materials is corrected. The assumption of variable permeability as a function of magnetic vector potential leads to:

$$\nabla \times \frac{1}{\mu} \nabla \times \vec{A} = -S \quad . \tag{2}$$

This equation is solved best numerically and the different numerical methods currently being used are given below in brief. Nonlinear successive overrelaxation is proposed by Schector[3] and discussed by Concus.[4] The method does not use permeability values in iron based on actual measurement data, but on the variational equation

$$I = \iint_R [\, g(|\vec{\nabla} A|^2) - 8\pi SA \,] \, dxdy \quad . \tag{3}$$

The magnetic vector potential $A(x,y)$, twice differentiable in the region R, should satisfy the assumed boundary condition and minimize the integral I in Eq. (3)

The function $g\,(|\vec{\nabla} A|^2)$ is proportional to the magnetostatic energy and is related to the permability by:

$$\frac{1}{\mu} = \frac{dg}{d(|\vec{\nabla} A|^2)} \quad . \tag{4}$$

The variational equation based on this assumption leads to:

$$\mu\ (|\vec{\nabla}A|^2) = \frac{1 + (|\vec{\nabla}A|^2)}{10^{-4} + (|\vec{\nabla}A|^2)} \quad . \tag{5}$$

A linearization of the nonlinear differential equation (2) and scaling the vector potential by:

$$C_m = \frac{\oint \vec{H}\, d\vec{\ell}}{(NI)_{applied}} \tag{6}$$

is reported by Ahmad.[5,6]

This method is suitable for magnets with low field strength where the flux density in iron is far from saturation. However, as a first guess it yields a good approximation to high field problems.

The method of solving Eq. (2) developed at SLAC in the code "NUTCRACKER" is to solve the quasi-Poisson Eq. (2) by successive overrelaxation of the magnetic vector potential and underrelaxation of the permeability in iron.

The method of Ahmad[5] is used in the SLAC code as an initial guess in order to reduce computation time. The outline of the SLAC computer code is described below.

In the case of variable permeability throughout the ferromagnetic body and double infinite symmetry, a quasi-Poisson equation of the form

$$\frac{\partial}{\partial x}\left(\frac{1}{\mu}\ \frac{\partial A_z}{\partial x}\right) + \frac{\partial}{\partial y}\left(\frac{1}{\mu}\ \frac{\partial A_z}{\partial y}\right) = -S_z \tag{7}$$

must be solved. The solution from the NUTCRACKER program uses Maxwell's equation:

$$\nabla \times \vec{H} = \vec{S} + \frac{\partial D}{\partial t} \tag{8}$$

with $\frac{\partial \vec{D}}{\partial r} = 0$

we get

$$\nabla \times \frac{1}{\mu} \nabla \times \vec{A} = \vec{S} \tag{9}$$

as the basis of our approach.

B. Derivation in Rectangular Coordinates

If $\hat{i}$, $\hat{j}$, and $\hat{k}$ are the unit vectors, doubly infinite symmetry may be expressed by the following two vector equations:

$$\vec{S} = S_z (x,z)\, \hat{k}, \tag{10}$$

and

$$\vec{A} = A_z (x,z)\, \hat{k} . \tag{11}$$

Equation (9) can be given in the form:

$$\nabla \times \frac{1}{\mu} \nabla \times \vec{A} = \begin{vmatrix} \hat{i} & \hat{j} & \hat{k} \\ \frac{\partial}{\partial x} & \frac{\partial}{\partial y} & \frac{\partial}{\partial z} \\ \frac{1}{\mu} \frac{\partial A_z}{\partial y} & -\frac{1}{\mu} \frac{\partial A_z}{\partial x} & 0 \end{vmatrix} \tag{12}$$

which, evaluated, is

$$\nabla \times \frac{1}{\mu} \nabla \times \vec{A} = \hat{i} \frac{\partial}{\partial z} \left(\frac{1}{\mu} \frac{\partial A_z}{\partial x} \right) + \hat{j} \frac{\partial}{\partial z} \left(\frac{1}{\mu} \frac{\partial A_z}{\partial y} \right) - \hat{k} \left[\frac{\partial}{\partial x} \left(\frac{1}{\mu} \frac{\partial A_z}{\partial x} \right) + \frac{\partial}{\partial y} \left(\frac{1}{\mu} \frac{\partial A_z}{\partial y} \right) \right]. \tag{13}$$

As $\vec{A}$ is independent of z,

$$\frac{\partial}{\partial z}\left[\frac{1}{\mu}\ \frac{\partial A_z}{\partial x}\right] = \frac{\partial}{\partial z}\left[\frac{1}{\mu}\ \frac{\partial A_z}{\partial y}\right] = 0$$

we get:

$$\nabla \times \frac{1}{\mu}\ \nabla \times \vec{A} = -\hat{k}\left[\frac{\partial}{\partial x}\left(\frac{1}{\mu}\ \frac{\partial A_z}{\partial x}\right) + \frac{\partial}{\partial y}\left(\frac{1}{\mu}\ \frac{\partial A_z}{\partial x}\right)\right]. \tag{14}$$

Combining Eqs. (9) and (14) yields,

$$\left[\frac{\partial}{\partial x}\left(\frac{1}{\mu}\ \frac{\partial A_z}{\partial y}\right) + \frac{\partial}{\partial y}\left(\frac{1}{\mu}\ \frac{\partial A_z}{\partial y}\right)\right]\hat{k} = -S_z\ \hat{k} \tag{15}$$

which is the quasi-Poisson equation for the magnetic vector potential as shown in Eq. (7).

C. Derivation in Cylindrical Coordinates

If $\hat{\epsilon}_1$, $\hat{\epsilon}_2$, and $\hat{\epsilon}_3$ are the base vectors in the cylindrical coordinate system, using the transformation equations from Cartesian to cylindrical coordinate, the curl of the vector potential can be given in the form:

$$\nabla \times \vec{A} = \begin{vmatrix} \frac{1}{r}\hat{\epsilon}_1 & \hat{\epsilon}_2 & \frac{1}{r}\hat{\epsilon}_3 \\ \frac{\partial}{\partial r} & \frac{\partial}{\partial \theta} & \frac{\partial}{\partial z} \\ 0 & rA_\theta & 0 \end{vmatrix}$$

and

$$\nabla \times \frac{1}{\mu} \nabla \times \vec{A} = \begin{vmatrix} \frac{1}{r}\hat{\epsilon}_1 & \hat{\epsilon}_2 & \hat{\epsilon}_3 \\ \frac{\partial}{\partial r} & \frac{\partial}{\partial \theta} & \frac{\partial}{\partial z} \\ -\frac{1}{\mu r} \cdot \frac{\partial}{\partial z}(rA_\theta) & 0 & \frac{1}{\mu r} \cdot \frac{\partial}{\partial r}(rA_\theta) \end{vmatrix} \quad (16)$$

which gives:

$$\nabla \times \frac{1}{\mu} \nabla \times \vec{A} = \frac{1}{r} \frac{\partial}{\partial \theta} \left(\frac{1}{\mu r} \frac{\partial}{\partial r}(rA_\theta) \right) \hat{\epsilon}_1 - \left\{ \frac{\partial}{\partial r} \left[\frac{1}{\mu r} \cdot \frac{\partial}{\partial r}(rA_\theta) \right] + \frac{\partial}{\partial z} \left[\frac{1}{\mu r} \frac{\partial}{\partial z}(rA_\theta) \right] \hat{\epsilon}_2 \right.$$

$$\left. + \frac{1}{\mu r} \frac{\partial}{\partial \theta} \left[\frac{1}{\mu r} \frac{\partial}{\partial z}(rA_\theta) \right] \hat{\epsilon}_3 \right\} . \quad (17)$$

As A_θ is independent of θ, Eq. (17) reduces to:

$$\nabla \times \frac{1}{\mu} \nabla \times \vec{A} = - \left\{ \frac{\partial}{\partial r} \left[\frac{1}{\mu r} \frac{\partial}{\partial r}(rA_\theta) \right] + \frac{\partial}{\partial z} \left[\frac{1}{\mu r} \frac{\partial}{\partial z}(rA_\theta) \right] \right\} \hat{\epsilon}_2 .$$

Combining Eqs. (9) and (17), we get

$$\frac{\partial}{\partial r} \left[\frac{1}{\mu r} \frac{\partial}{\partial r}(rA_\theta) \right] + \frac{\partial}{\partial z} \left[\frac{1}{\mu r} \frac{\partial}{\partial z}(rA_\theta) \right] = - S_\theta . \quad (18)$$

$S_\theta = S_\theta(r,z)$

II. COMPUTATION METHODS USED IN THE PROGRAM

When solving a partial differential equation by numerical methods, one discretizes the space and uses a finite difference approximation to the partial differential equation.

For linear equations, relaxation may be used with good results. Since the permeability is given by

$$\mu = \mu \left(\left| \nabla \times \vec{A} \, (x, y) \right| \right) \tag{19}$$

Eqs. (15) and (18) are not linear and a modification of the method of Ahmad[5,6] has been chosen.

The method of solving the partial differential equations given in Eqs. (15) and (18) is divided into two phases:

Phase I

(a) Overrelaxation of the magnetic vector potential in every point in the net using the finite different equivalent to Eq. (15) or Eq. (18).

(b) Calculation of the ratio

$$C_n = \frac{\iint \vec{S} \cdot d\vec{s}}{\int \vec{H} \cdot d\vec{\ell}} \tag{20}$$

and scaling potential values in the net by C_n if appropriate.

(c) Underrelaxation of the permeability at each point in the net.

Phase I linearized the problem. Its convergence is speeded up by a factor of 5 to 10 compared to other methods, and fairly accurate results are obtained, as will be shown later.

Phase II

In this Phase the solution proceeds as follows:

(a) Successive overrelaxations of every vector potential value in the mesh,

(b) The simultaneous underrelaxation of every permeability corresponding to a specific potential value.

If Phase I of the solution is used, we observe that after 30-50 iterations the convergence rate is slowed down. This can be seen by examining the magnitude of the absolute value of residuals, which either remain constant, or oscillate around some fixed value.

At this time Phase II begins to operate and the solution starts to converge to any set value and accuracy desired.

A. Successive Overrelaxation

The vector potential at any point in space may be expressed by a linear combination of m adjoining points. The general form of the equation is:

$$A_o = \sum_{i=1}^{m} C_i A_i \tag{21}$$

with A_o as the vector potential at an arbitrary point in the net. If superscripts denote the number of iterations in Eq. (21), we rewrite the equation:

$$A_o^{n+\frac{1}{2}} = \sum_{i=1}^{m} C_i A_i^n \tag{22}$$

The overrelaxation equation is then

$$A_o^{n+1} = (1-\omega)\ A_o^n + \omega A_o^{n+\frac{1}{2}} \tag{23}$$

for

$$1 < \omega < 2 \quad .$$

Equation (23) is applied to each net point successively.

Now if p and q denote the number of nodes in the x and y directions for a specific net, we may write as a good approximation[7]:

$$\omega = 2 - \pi\sqrt{2}\left[\frac{1}{p^2} + \frac{1}{q^2}\right]^{\frac{1}{2}} \tag{24}$$

for $p > 15, \; q > 15$.

B. Acceleration of Convergence

Acceleration of convergence is achieved by scaling the vector potential throughout the area s_m by a factor C_m, defined as:

$$C_m = \frac{\iint \vec{S}\, d\vec{s}}{\oint \vec{H} d\vec{\ell}} \quad . \tag{25}$$

Equation (25) is a modification of Ampere's law:

$$\oint \vec{H}\, d\vec{\ell} = \iint \vec{S}\, d\vec{s} \quad . \tag{26}$$

The number of ampere-turns used as initial input in the system determines $\iint \vec{S}\, d\vec{s}$ but $\oint \vec{H} d\vec{\ell}$ is calculated separately using $\nabla \times \vec{A}$ and the numerical values of the vector potential.

If the calculated values of H are too large, C_m will be smaller than unity ($C_m < 1$) and the potentials are automatically reduced, carrying a drop in $\nabla \times \vec{A}$ and hence in $\oint \vec{H} d\vec{\ell}$.

Ideally C_m should be unity, but numerous difficulties arise due to oscillation around the true solution and $C_m = 1$ is hardly ever achieved. It may be seen that as the computation progresses, C_m will vary in the region $0.96<C<1.04$ for most problems solved.

After each SOR* the line integral of field intensity is integrated around a suitable path. If $0.01 \leq C_m \leq 100$, the potential values are multiplied by C_m. One may choose several paths for line integrals and use a different C_m for each integral.

C. Underrelaxation of Permeabilities

Due to the non-linear properties of μ, the overrelaxation Eq. (23) was not applied for μ. Instead we used:

$$\mu^{n+1} = (1 - \omega_\mu)\, \mu^n + \omega_\mu \mu^{n+1/2}, \tag{27}$$

where μ^n is the value of permeability, after the n-th iteration, at some point in the net. The term $\mu^{n+1/2}$ is obtained from measured permeability curves suitably fitted for the program.

If the μ-H curve is represented by G_μ [see Fig. (8)], then

$$\mu^{n+1/2} = G_\mu \left(\frac{\nabla \times \vec{A}^{n+1} \cdot \nabla \times \vec{A}^{n+1}}{\mu^n} \right) . \tag{28}$$

Empirically ω_μ is found to be about 0.15 to 0.25. For each point in the net a new permeability μ^{n+1} is calculated.

---

*SOR = Successive over relaxation.

D. Convergence Test

To judge how close one has come to the true solution has been always a difficult task. Binns[8] gives a few practical criteria for satisfactory solutions, which have been applied in the NUTCRACKER program:

(a) The residual of each mode is less than 0.1% of the mean potential value.

(b) The algebraic sum of all residuals is of the same order of magnitude as each residual.

(c) The residuals are "uniformly mixed" with regard to sign and magnitude over the whole region.

Criteria (a) and (c), although very important, are rather time consuming, if applied to the computer program. At any iteration there are actually four solutions to the problem:

(1) The "true" or actually measured values of the field after the magnet is tested.

(2) The analytic solution to the quasi-Poisson equation with imposed boundary values.

(3) The solution of the finite difference equation as an approximation to the partial differential equation (which occurs when all residuals are zero).

(4) The solution to the finite difference equation after n iterations.

A good approach is to express (4) in terms of (3).

Binns[8] gives a solution for a five-node molecule:

$$\delta_n = \frac{R_n \cdot \rho^2}{4h^2} \tag{29}$$

with δ_n = a measure of the error,

R_n = maximum residual at the end of the n-th iteration

ρ = radius of a circle, which contains the field region.

The program switches from Phase I to Phase II when $\delta_n \leq \delta_I$ and $\left|1 - C_m\right| < 0.05$.

If $\delta_n \leq \delta_{II}$, then Phase II is complete and the magnetic field, the vector potential, and the permeability values are printed for any mesh point in the network.

Both δ_I and δ_{II} are specified in the program.

III. FINITE DIFFERENCE EQUATIONS IN RECTANGULAR COORDINATES

The finite difference approximation to Eq. (15) is obtained to the continuous function $A_z(x,y)$ by a discrete function A. The correspondence between $A_z(x,y)$ and A with respect to an arbitrary point (x,y) is given by the following six expressions:

$$\begin{aligned} A_z(x,y) &= A_O \ , \\ A_z(x+h,y) &= A_E \ , \\ A_z(x-h,y) &= A_W \ , \\ A_z(x,y+h) &= A_N \ , \\ A_z(x,y-h) &= A_S \ , \\ A_z(x,y+2h) &= A_{NN} \ . \end{aligned} \tag{30}$$

The discrete function is represented graphically in Fig. 1. Points midway between the nodes are noted by subscripts.

The first partial derivatives, multiplied by the inverse permeability between nodes, are approximated by:

$$\left[\frac{1}{\mu}\ \frac{\partial A_z}{\partial x}\right]_1 \doteq \left(\frac{\frac{1}{\mu_O} + \frac{1}{\mu_E}}{2}\right)\left(\frac{A_E - A_O}{h}\right) \ , \tag{31}$$

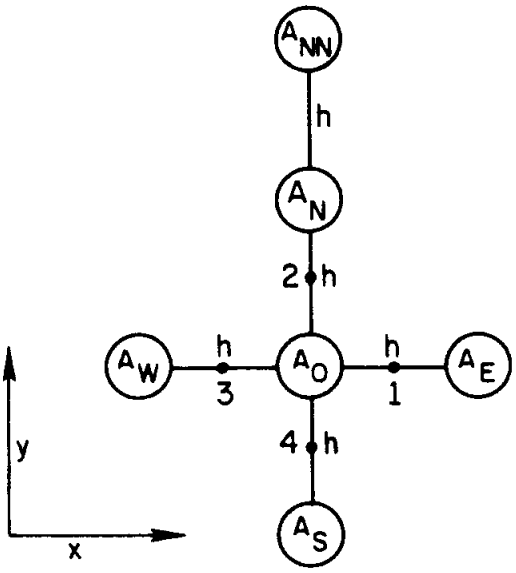

FIG. 1 -- DISCRETE VECTOR POTENTIAL IN RECTANGULAR COORDINATES.

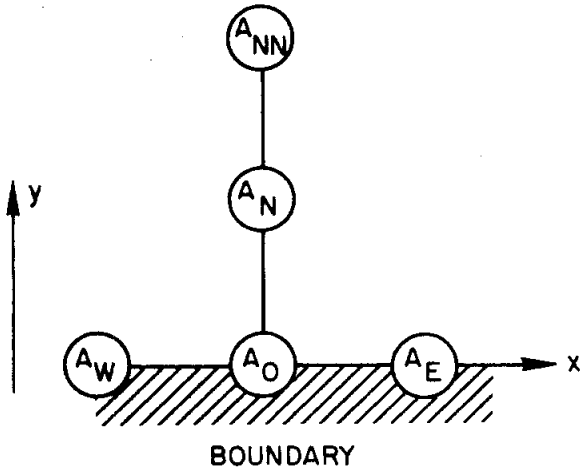

FIG. 2 -- DISCRETE VECTOR POTENTIAL.

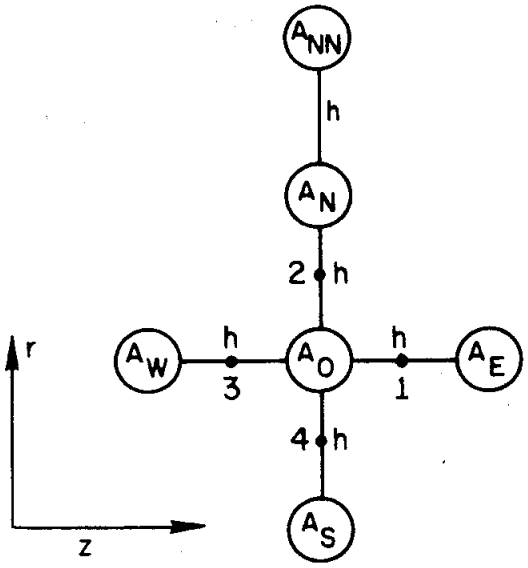

FIG. 3 -- DISCRETE VECTOR POTENTIAL IN CYLINDRICAL COORDINATES.

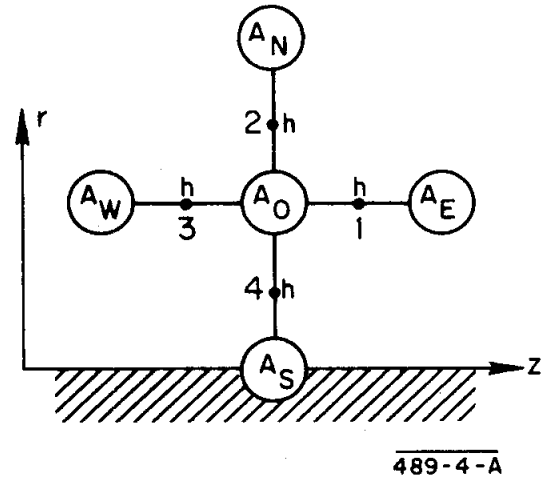

FIG. 4 -- DISCRETE VECTOR POTENTIAL ON THE AXIS OF SYMMETRY.

$$\left[\frac{1}{\mu}\frac{\partial A_z}{\partial x}\right]_3 \doteq \left(\frac{\frac{1}{\mu_O}+\frac{1}{\mu_W}}{2}\right)\left(\frac{A_O - A_W}{h}\right) , \tag{32}$$

$$\left[\frac{1}{\mu}\frac{\partial A_z}{\partial y}\right]_2 \doteq \left(\frac{\frac{1}{\mu_O}+\frac{1}{\mu_N}}{2}\right)\left(\frac{A_N - A_O}{h}\right) , \tag{33}$$

$$\left[\frac{1}{\mu}\frac{\partial A_z}{\partial y}\right]_4 \doteq \left(\frac{\frac{1}{\mu_O}+\frac{1}{\mu_S}}{2}\right)\left(\frac{A_O - A_S}{h}\right) . \tag{34}$$

The second derivatives at each center node are approximated by

$$\frac{\partial}{\partial x}\left(\frac{1}{\mu}\frac{\partial A_z}{\partial y}\right)_O \doteq \frac{1}{2h^2}\left[\left(\frac{1}{\mu_O}+\frac{1}{\mu_E}\right)\left(A_E - A_O\right) - \left(\frac{1}{\mu_O}+\frac{1}{\mu_W}\right)\left(A_O - A_W\right)\right] , \tag{35}$$

$$\frac{\partial}{\partial y}\left(\frac{1}{\mu}\frac{\partial A_z}{\partial y}\right)_O \doteq \frac{1}{2h^2}\left[\left(\frac{1}{\mu_O}+\frac{1}{\mu_W}\right)\left(A_W - A_O\right) - \left(\frac{1}{\mu_O}+\frac{1}{\mu_S}\right)\left(A_O - A_S\right)\right] . \tag{36}$$

Replacing the left-hand side of Eq. (15) by the finite difference approximations and solving for A_O, one obtains

$$A_O = \frac{\left(\frac{1}{\mu_N}+\frac{1}{\mu_O}\right)A_N + \left(\frac{1}{\mu_S}+\frac{1}{\mu_O}\right)A_S + \left(\frac{1}{\mu_E}+\frac{1}{\mu_O}\right)A_E + \left(\frac{1}{\mu_W}+\frac{1}{\mu_O}\right)A_W + 2h^2 S_O}{\frac{1}{\mu_N}+\frac{1}{\mu_S}+\frac{1}{\mu_E}+\frac{1}{\mu_W}+\frac{4}{\mu_O}} . \tag{37}$$

Equation (37) represents the finite difference equation to be satisfied by the successive overrelaxation methods discussed in Sec. II.

A. Magnetic Field Intensity in Rectangular Coordinates

The magnetic field intensity is obtained from the finite difference solution by an approximation to the curl. Recalling that

$$\vec{H} = \frac{1}{\mu} \nabla \times A_z \, \hat{k} \quad , \tag{38}$$

we may express the magnetic field intensity in rectangular coordinates as

$$\vec{H} = \frac{1}{\mu} \left[\frac{\partial A_z}{\partial y} \, \hat{i} - \frac{\partial A_z}{\partial x} \, \hat{j} \right] . \tag{39}$$

Thus, at the center node, $\vec{H}$ is given by

$$\vec{H} = \frac{1}{\mu_o} \left[\frac{A_N - A_S}{h} \, \hat{i} - \frac{A_E - A_W}{h} \, \hat{j} \right] . \tag{40}$$

On the boundary (see Fig. 2) the field is given by the equation

$$\vec{H} = \frac{1}{\mu_o} \left[\frac{-3A_o + 4A_N - A_{NN}}{2h} \, \hat{i} - \frac{A_E - A_W}{2h} \, \hat{j} \right] . \tag{41}$$

The numerical approximation to $\frac{\partial A}{\partial y}$ at $y=0$ is given by Salvadors and Baron.[9]

IV. FINITE DIFFERENCE EQUATIONS IN CYLINDRICAL COORDINATES

As in the case of rectangular coordinates, a continuous function is usually approximated by a discrete function. This approximation is represented graphically in Fig. 3.

With respect to an arbitrary point (r,z) the correspondence between $\vec{A}$ and the approximation is expressed in Eqs. (42).

$$\begin{aligned} A_\theta\ (r,z) &= A_O\ , \\ A_\theta\ (r+h,z) &= A_N\ , \\ A_\theta\ (r-h,z) &= A_S\ , \\ A_\theta\ (r,z+h) &= A_E\ , \\ A_\theta\ (r,z-h) &= A_W\ , \\ A_\theta\ (r,z+2h) &= A_{NN}\ . \end{aligned} \tag{42}$$

The first partial derivatives multiplied by the inverse value of permeability times radial distance are

$$\left[\frac{1}{\mu r}\frac{\partial}{\partial z}(rA_\theta)\right]_1 \doteq \left(\frac{\frac{1}{\mu_E r_E}+\frac{1}{\mu_O r_O}}{2}\right)\left(\frac{r_E A_E - r_O A_O}{h}\right) \tag{43}$$

$$\left[\frac{1}{\mu r}\frac{\partial}{\partial r}(rA_\theta)\right]_2 \doteq \left(\frac{\frac{1}{\mu_N r_N}+\frac{1}{\mu_O r_O}}{2}\right)\left(\frac{r_N A_N - r_O A_O}{h}\right) \tag{44}$$

$$\left[\frac{1}{\mu r}\frac{\partial}{\partial z}(rA_\theta)\right]_3 \doteq \left(\frac{\frac{1}{\mu_O r_O}+\frac{1}{\mu_W r_W}}{2}\right)\left(\frac{r_O A_O - r_W A_W}{h}\right) \tag{45}$$

$$\left[\frac{1}{\mu r}\frac{\partial}{\partial z}(rA_\theta)\right]_4 \doteq \left(\frac{\frac{1}{\mu_O r_O}+\frac{1}{\mu_S r_S}}{2}\right)\left(\frac{r_O A_O - r_S A_S}{h}\right). \tag{46}$$

The second partial derivatives at the center node are respectively

$$\left[\frac{\partial}{\partial r}\left(\frac{1}{\mu r}\frac{\partial}{\partial r}(rA_\theta)\right)\right]_0$$

$$= \frac{1}{2h^2}\left[\left(\frac{1}{\mu_N r_N}+\frac{1}{\mu_O r_O}\right)\left(r_N A_N - r_O A_O\right) - \left(\frac{1}{\mu_O r_O}+\frac{1}{\mu_S r_S}\right)\left(r_O A_O - r_S A_S\right)\right] \tag{47}$$

and

$$\left[\frac{\partial}{\partial z}\left(\frac{1}{\mu r}\frac{\partial}{\partial z}(rA_\theta)\right)\right]_0$$

$$= \frac{1}{2h^2}\left[\left(\frac{1}{\mu_E r_E}+\frac{1}{\mu_O r_O}\right)\left(r_E A_E - r_O A_O\right) - \left(\frac{1}{\mu_O r_O}+\frac{1}{\mu_W r_W}\right)\left(r_O A_O - r_W A_W\right)\right]. \quad (48)$$

Replacing the left-hand side of Eq. (18) with the approximations to the second partial derivatives and solving for A_O, one obtains

$$A_O = \frac{\left(\frac{1}{\mu_N r_N}+\frac{1}{\mu_O r_O}\right) r_N A_N + \left(\frac{1}{\mu_S r_S}+\frac{1}{\mu_O r_O}\right) r_S A_S + \left(\frac{1}{\mu_E r_E}+\frac{1}{\mu_O r_O}\right) r_E A_E + \left(\frac{1}{\mu_W r_W}+\frac{1}{\mu_O r_O}\right) r_W A_W + 2h^2 S_\theta}{r_O\left(\frac{1}{\mu_N r_N}+\frac{1}{\mu_S r_S}+\frac{1}{\mu_E r_E}+\frac{1}{\mu_W r_W}+\frac{4}{\mu_O r_O}\right)} \quad (49)$$

The iterative solution to Eq. (49) is the z-axially symmetric magnetic vector potential in cylindrical coordinates.

On the axis of symmetry, the magnetic vector potential is zero. One mesh unit away from the axis (see Fig. 4), Eq. (49) must be void of poles; with $r_E = r_W = r_O = h$, $r_N = 2h$, and $r_S = 0$, Eq. (49) becomes

$$A_O = \frac{\frac{4}{3}\left(\frac{1}{\mu_N}+\frac{1}{\mu_O}\right) A_N + \left(\frac{1}{\mu_E}+\frac{1}{\mu_O}\right) A_E + \left(\frac{1}{\mu_W}+\frac{1}{\mu_O}\right) A_W + 2h^2 S_\theta}{\frac{2}{3\mu_N}+\frac{2}{\mu_S}+\frac{1}{\mu_E}+\frac{1}{\mu_W}+\frac{14}{3\mu_O}} \quad . \quad (50)$$

A. The Magnetic Field Intensity in Cylindrical Coordinates

The magnetic field intensity is given by

$$\vec{H} = \frac{1}{\mu}\nabla \times A_\theta \hat{\epsilon}_2 \quad (51)$$

or,

$$\vec{H} = \frac{1}{\mu}\left[-\frac{\partial A_\theta}{\partial z}\cdot\hat{\epsilon}_1 + \frac{1}{r}\frac{\partial}{\partial r}(rA_\theta)\,\hat{\epsilon}_3\right] . \qquad (52)$$

The finite difference approximation to H at the center node in Fig. 3 is therefore:

$$\vec{H} = \frac{1}{2\mu_O}\left(\frac{A_E - A_W}{h}\right)\hat{\epsilon}_1 + \frac{1}{2\mu_O r_O}\left(\frac{r_N A_N - r_S A_S}{h}\right)\hat{\epsilon}_3 . \qquad (53)$$

At $r = 0$, $\vec{H}$ is obtained by the limiting process and L'Hospital's rule. The field intensity is then

$$\vec{H} = -\frac{1}{\mu}\frac{\partial A_\theta}{\partial z}\,\hat{\epsilon}_1 + \frac{2}{\mu}\frac{\partial A_\theta}{\partial r}\,\hat{\epsilon}_3 . \qquad (54)$$

In finite difference form it may be expressed as:

$$H = -\frac{1}{2\mu_O}\left(\frac{A_E - A_W}{h}\right)\hat{\epsilon}_1 + \frac{1}{\mu_O}\left(\frac{-3A_O + 4A_N - A_{NN}}{h}\right)\hat{\epsilon}_3 . \qquad (55)$$

V. GENERAL CONSIDERATIONS

A. Two-Dimensional Problems and Boundary Considerations

Three-dimensional magnetic configurations are reduced to two-dimensional problems by assuming symmetry conditions in one dimension.

In rectangular Cartesian coordinates, one usually assumes doubly infinite symmetry, i.e., the magnetic vector potential is independent of the z coordinate (see Fig. 5).

In axially symmetric cases, the magnetic vector potential is independent of the θ coordinate (Fig. 6).

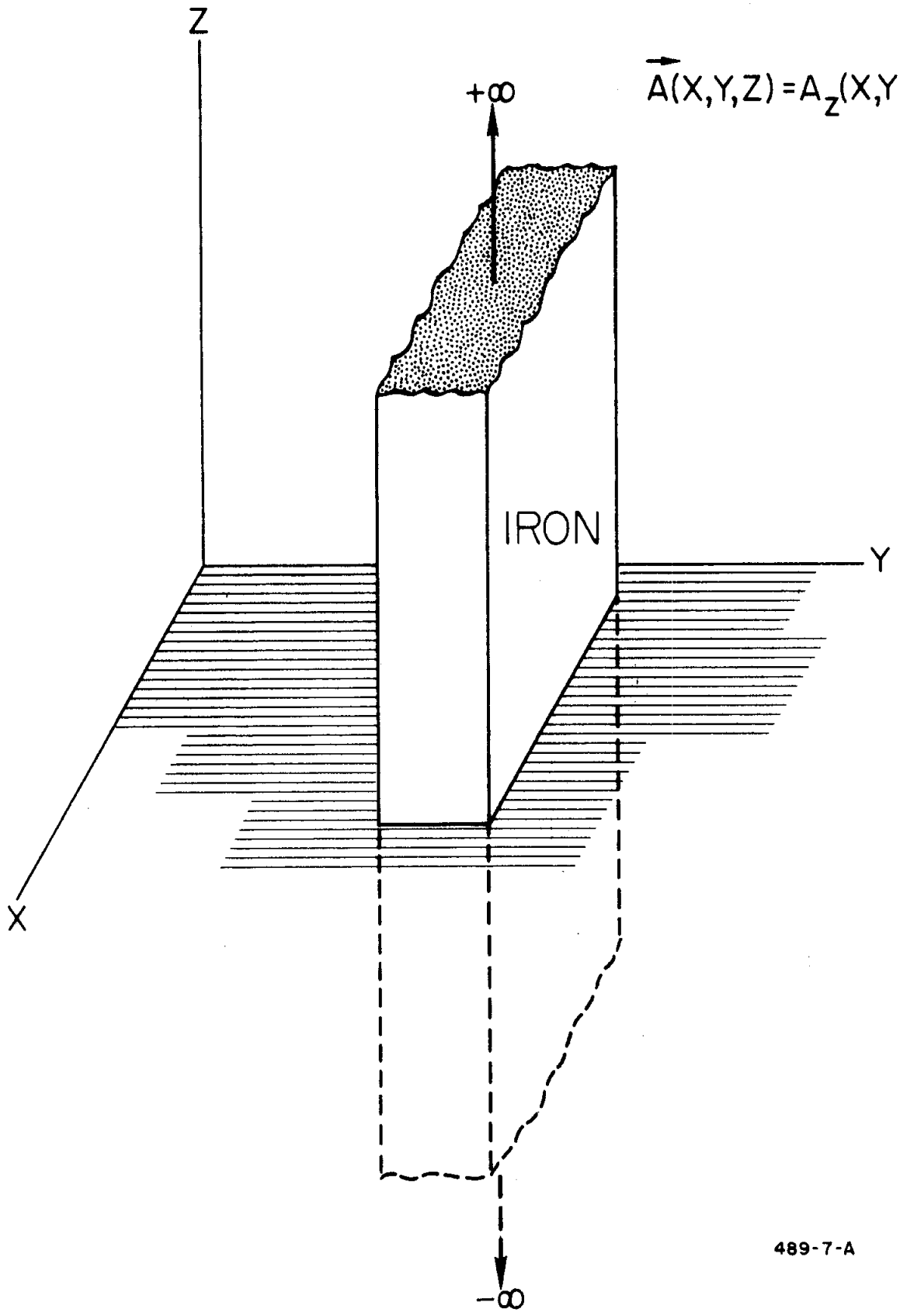

FIG. 5 - DOUBLY INFINITE SYMMETRIC CASE

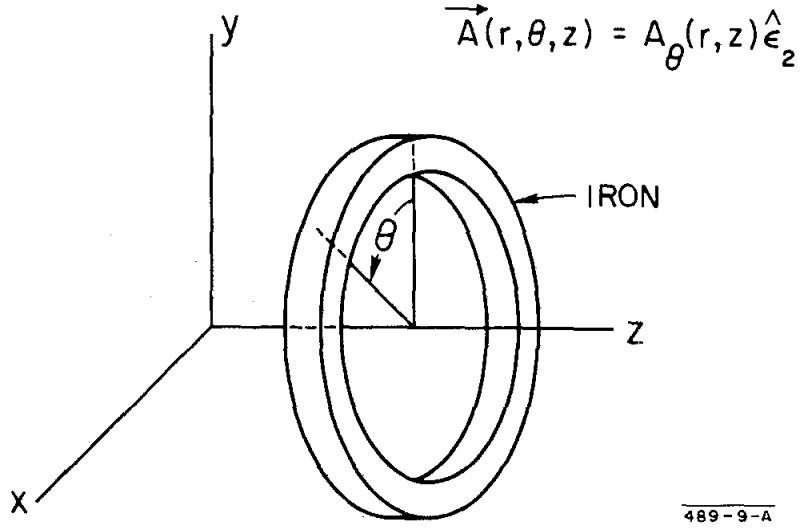

FIG. 6-- AXIALLY SYMMETRIC CASE

A futher reduction in a two-dimensional case will take place in rectangular coordinates in the form of a two-dimensional anti-symmetric problem (see Fig. 7), where the x-z plane is the surface of zero magnetic vector potential. When this condition is applied to finite difference equations, special consideration must be given to the x-axis ($z = 0$, $y = 0$).

Consider the molecule with the center node on the x-axis; then, anti-symmetry requires that $A_N = -A_S$ and $A_E = A_W = A_O = 0$.

The x-axis is chosen as a boundary and a line of zero potential. The flux density is parallel to the x-axis because

$$B_x = \frac{\partial A}{\partial y} = \frac{A_N - (-A_N)}{2h} = \frac{A_N}{h} \quad , \tag{56}$$

and

$$B_y = -\frac{\partial A}{\partial x} = 0 \quad . \tag{57}$$

In the case of axial symmetry, hyper-rectangular shapes with two square faces are usually used.

The magnetic vector potential along the z-axis is $A_\theta(0,z) = 0$.

B. Potential Boundaries

A magnetic system to be approximated by the method stated in this paper is enclosed in a rectangular area.

The magnetic vector potential is assumed to be zero or a constant along this boundary. An alternative assumption would allow Neumann conditions or the specification of Cauchy conditions. Newmann conditions require that the tangential flux component be zero and Cauchy conditions may add considerable computing time.

$$-A_z(x,y) = A_z(x,-y)$$

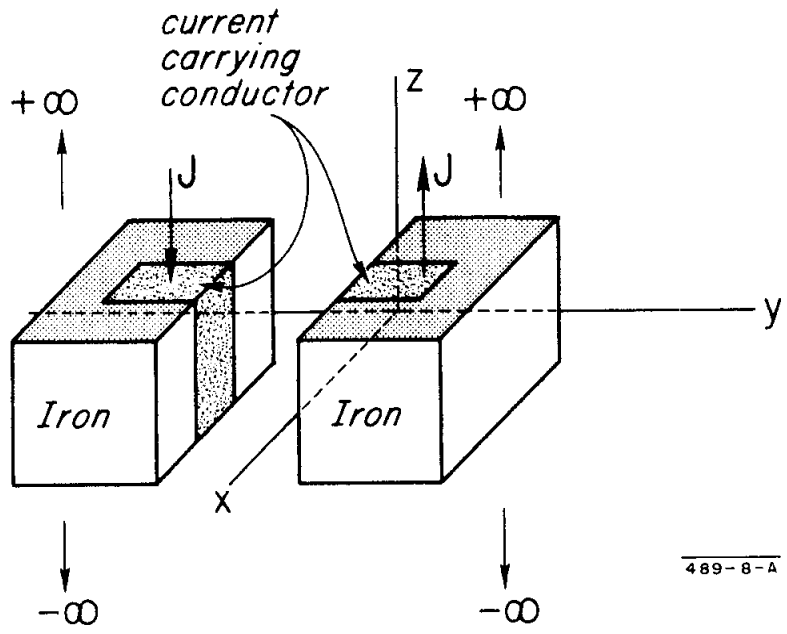

FIG. 7-- ANTISYMMETRIC-DOUBLY INFINITE SYMMETRY

C. Flux Density in Iron-Air Boundaries

Several approaches to the specification of boundary values were investigated.

1. Internal Conditions

From elementary theory, the relationships between B and H across an interface are (Fig. 8)

$$B_{1N} = B_{2N}$$

$$H_{1T} = H_{2T},$$

where the subscripts refer to the normal and tangential components of the field. In terms of the angles α_1 and α_2, these conditions become

$$B_1 \cos \alpha_1 = B_2 \cos \alpha_2 , \tag{58}$$

$$\frac{1}{\mu_0} B_1 \sin \alpha_1 = \frac{1}{\mu_{Fe}} B_2 \sin \alpha_2 . \tag{59}$$

Dividing Eq. (59) by Eq. (58), one obtains

$$\mu_{Fe} \tan \alpha_1 = \mu_0 \tan \alpha_2, \text{ and}$$

$$\tan \alpha_2 = \frac{1}{\mu_{r_{Fe}}} \tan \alpha_1 .$$

2. External Boundary Conditions

These conditions may be of three types:

(a) Dirichlet conditions, $A = g(x,y)$,

(b) Neumann conditions, $\frac{\partial A}{\partial n} = f(x,y)$ and

(c) Cauchy conditions, either $\frac{\partial A}{\partial n}$ or A specified.

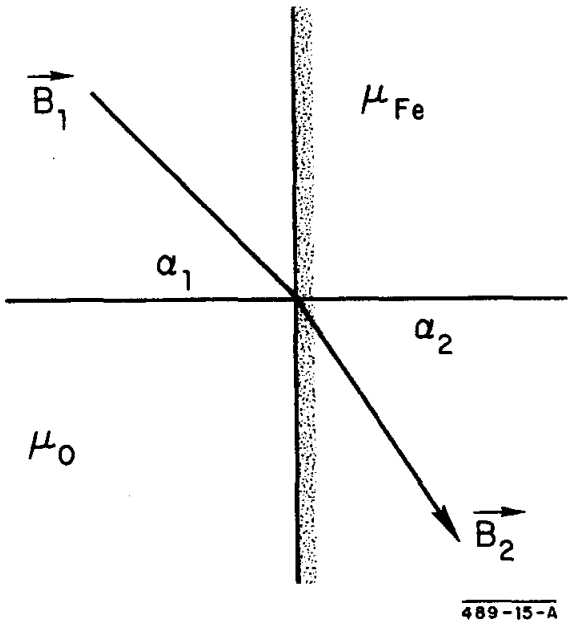

FIG. 8 -- FLUX DENSITY ACROSS BOUNDARIES

The best approach would be to use any one of these three types where appropriate. To do this, however, raises very complicated programming problems and it is found that type (a) is easiest to employ.

By using the Dirichlet condition $A = 0$ on our problems and allowing about four nodes of air between the iron and this boundary, we achieved reasonable results. For example, the internal conditions (a) were examined to see if they held in the region of the pole face. An angular discrepancy of about 1^{o} was found.

D. μ-H Curve

The nonlinear aspect of the quasi-Poisson equation is due to the variation of μ with H. An accurate functional form for this relationship was found by a curve-fitting program which incorporated data from a number of sources.

Throughout the lower portion of the μ-H curve, a function with a small additive term was quite satisfactory for expressing μ in terms of H. In the region $H < 700$ amp-meter^{-1} and $H > 28,000$ amp-meter^{-1} the data are subject to a wide margin of error. The μ-H curve is very critical for large H, due to the saturation effects in iron. Our best fits in these regions were linear and adjusted to make the entire curve continuous in the following manner:

The magnetization curve for ferromagnetic materials is expressed as

$$B = 4\pi M + \mu_o H , \tag{60}$$

with $4\pi M = 2.1$ volts/meter^2 the saturation value. The relative permeability is calculated from the expression:

$$\mu - 1 = \frac{4\pi M}{\mu_o H} . \tag{61}$$

For various H values the permeability values are fitted from the magnetization curve by the following expressions:

$$0 \leq H \leq 250 \text{ amps}\cdot\text{meter}^{-1} \qquad \mu = (250 + 7H)\,\mu_0 \tag{62}$$

$$250 < H \leq 350 \text{ amps}\cdot\text{meter}^{-1} \qquad \mu = 2000\,\mu_0 \tag{63}$$

$$350 < H < 700 \text{ amps}\cdot\text{meter}^{-1} \qquad \mu = 2000 - 1.868\,(H-350)\,\mu_0 \tag{64}$$

$$700 \leq H \leq 28,000 \text{ amps}\cdot\text{meter}^{-1} \qquad \mu = \frac{1.7088}{\left[\exp\left(\frac{333-H}{354}\right) + 1.243\,H\right]} + 4.31\times 10^{-3}\sqrt{H} \tag{65}$$

$$28,000 < H \text{ amps}\cdot\text{meter}^{-1} \qquad \mu = \frac{\mu(28,000)\times 28,000}{H} + \mu_0 \,.^{*} \tag{66}$$

Experimental data for B and μ values are shown in Fig. 9.

The convergence of the problem is definitely affected by the shape of the magnetization curve. The regions of the magnet where μ changes rapidly with H are relatively unstable during the initial iterations of the problem.

E. Lines of Equal Vector Potential

The interpretation of data from a two-dimensional problem, due to the sheer bulk, presents a problem. To circumvent this, contour plots of equal vector potential are usually presented.

Consider a curve $C : y = y(x)$ in two-dimensional space along which the vector potential $\vec{A}$ is constant. $\vec{A}$ is represented parametrically with respect to x, by

$$\vec{A}\,(x,y) = A_z[x, y(x)] \,. \tag{67}$$

---

* $\mu(28,000)$ is the value of μ for $H = 28,000$. This is done by recursion in the computer program.

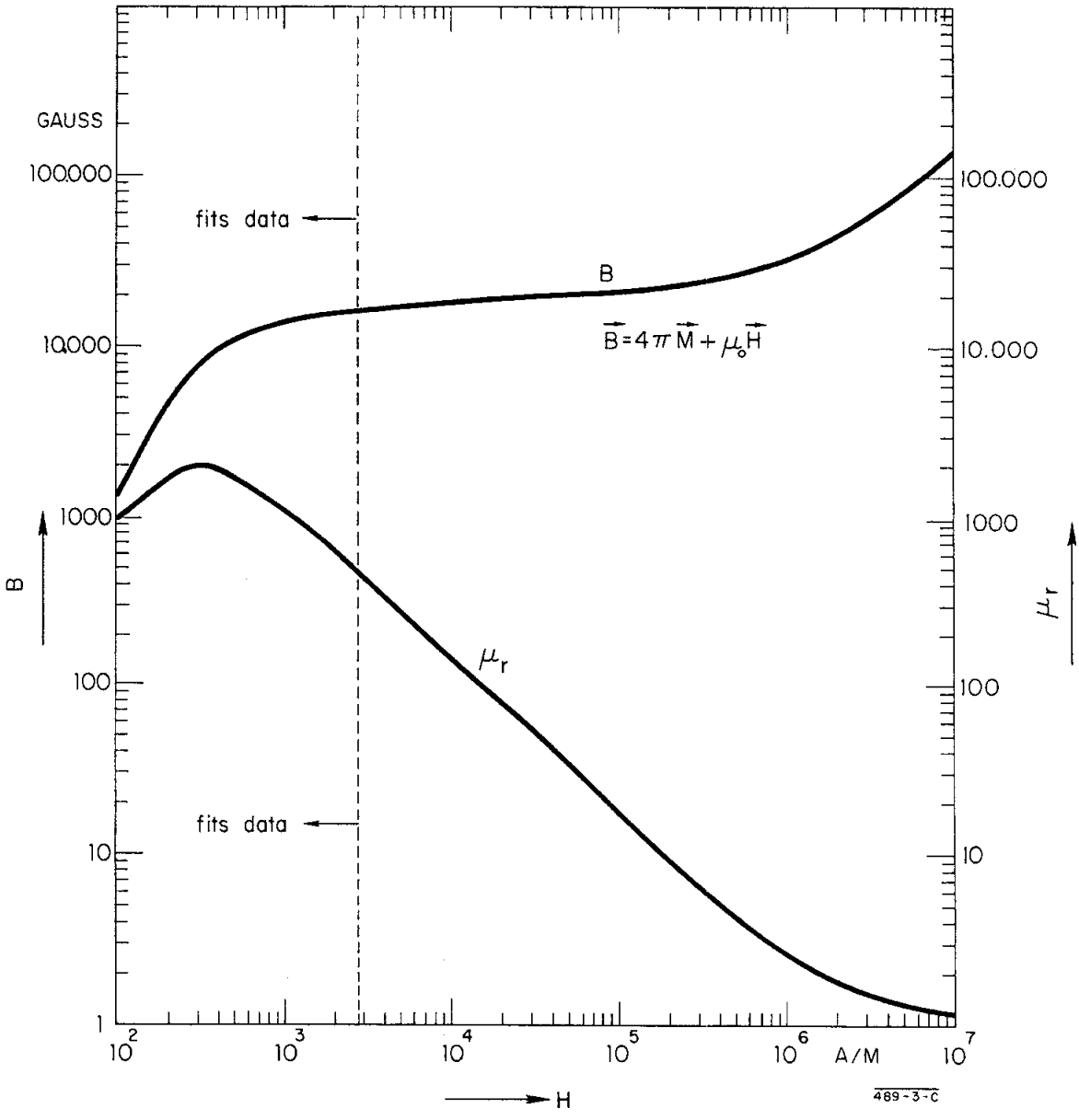

Fig. 9-B AND μ CURVES FILLED TO MEASURED DATA

Since $\vec{A}$ is constant in magnitude along C, one has

$$dA_z = \frac{\partial A_z}{\partial x} dx + \frac{\partial A_z}{\partial y} dy = 0 \quad . \tag{68}$$

Now

$$B_x = \frac{\partial A_z}{\partial y} \text{ and } B_y = -\frac{\partial A_z}{\partial x} \; ; \tag{69}$$

thus

$$-B_y dx + B_x dy = 0 \quad . \tag{70}$$

Therefore, the slope of the curve C represents the tangent of the angle of the flux density. This may be seen by the following equation:

$$\frac{dy}{dx} = \frac{B_y}{B_x} \quad . \tag{71}$$

In cylindrical coordinates, one is concerned with a curve where $r\vec{A}(r,z)$ is constant in magnitude. Consider $d(rA_\theta) = 0$ along the curve C; the obvious conclusion then is $\frac{dr}{dz} = \frac{B_r}{B_z}$.

F. Current Distribution

The current density over the entire coil cross section is assumed to be uniform. The effect of conductor shape, cooling passages, and insulation is taken into account by introducing a space factor λ.

Thus the basic assumption on the current density $\vec{S}$, over a rectangular cross-sectional s, is

$$\vec{S}(x,y) = \lambda S \hat{k}, \quad (x,y) \in s \quad \text{or} \quad \vec{S}(r,z) = \lambda S \hat{\epsilon}_2, \quad (r,z) \in s .$$

G. Practical Applications of the Mathematical Model

The analysis and computer code were undertaken to solve general magnetic problems which are encountered in the design of large magnets.

As in most systems, pure symmetry cannot be expected, because of the shapes and requirements on the various types of magnets. However, approximations to pure symmetry have been used in a 2-meter spark chamber magnet,[10] and in the SLAC 1-meter bubble chamber magnet. Model measurements have shown that an accuracy better than 5% between calculations and measurement had been achieved for the spark chamber magnet with axial symmetry.

The approximation of a beam transport magnet[11] in a two-dimensional configuration is shown in the next section.

VI. COMPARISON OF CALCULATION AND MEASUREMENTS FOR THE SLAC 3° BENDING MAGNET

To determine the efficiency and accuracy of the NUTCRACKER program, the SLAC 3° bending magnet shown in Fig. 10 was recalculated. Experimental data at various flux densities in the gap were available. The calculation assumed doubly infinite symmetry, and magnetization curves were obtained experimentally for pure ingot iron containing 0.08% carbon and 0.1% Si in the ladle analysis.

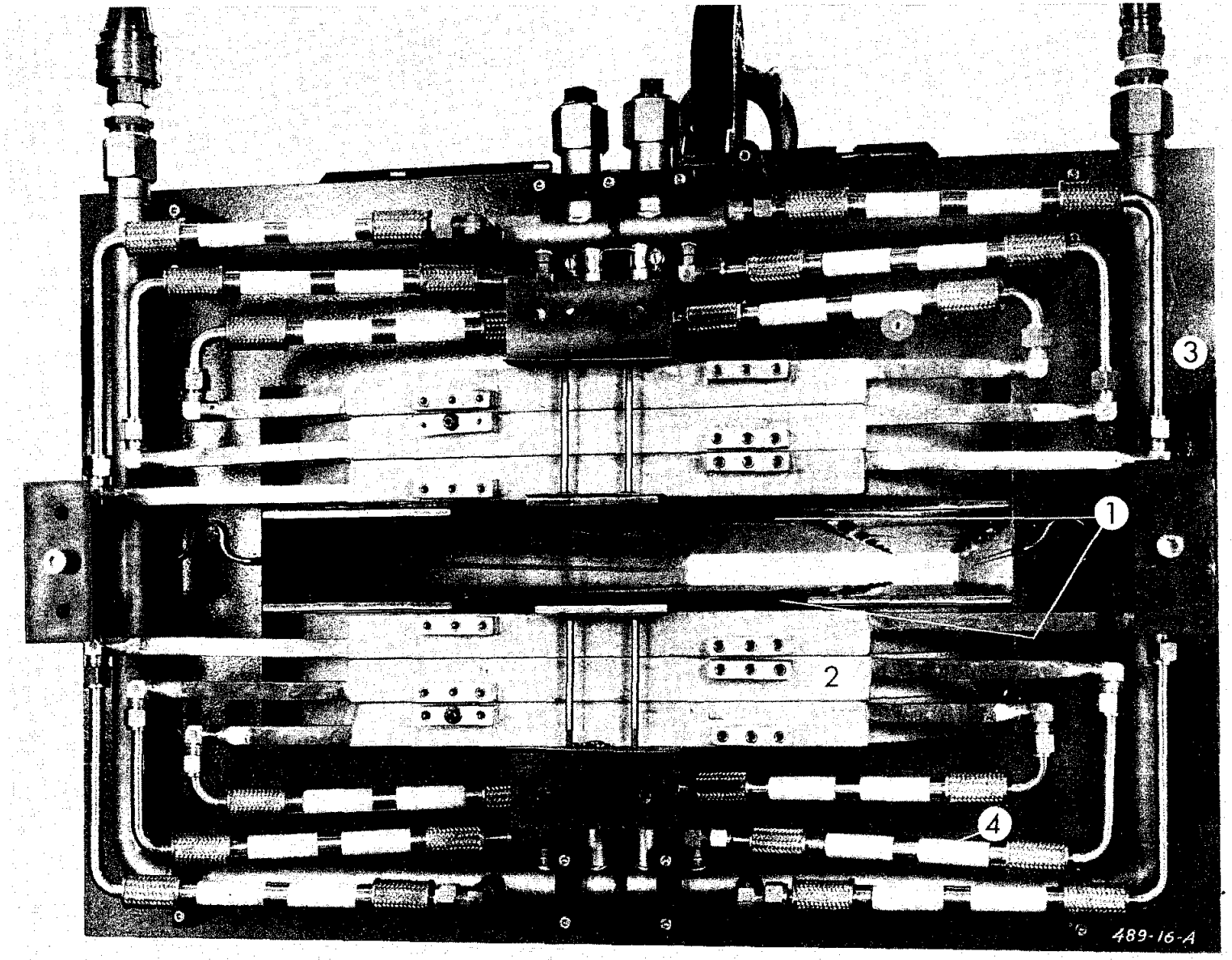

FIG. 10 - SLAC 3° BENDING MAGNET

1. Pole tips
2. Coil
3. Iron return yoke
4. Ceramic stainless steel water connection

Symmetry in the x-y plane allows us to consider only half of the magnet. Figure 11 shows the distribution of the nodes, where each mark is the center of a 1×1 cm^2 mesh. The boundary line with $A = 0$ is assumed arbitrarily, primarily due to computer limitations. In our case the B 5500 computer was used. The print-outs of the equipotential lines and the relative permeability lines are shown in Figs. 12 and 13. The measured and calculated y component of the flux density along the median plane and 1 cm below the pole surface is given in Figs. 14–16.

As mentioned previously, the NUTCRACKER program is still not usable for curved boundaries; however, a 45° line approximating the shimming at the pole ends is assumed for calculation.

At the pole center the calculated maximum field value is 14.35 kG, which may be compared with the measured value of 14.5 kG. The maximum deviation occurs at the pole ends due to the assumption of the 90° pole edge in our calculation. The deviation 1 cm below the pole surface is 1.5% at the pole ends and the fall-off of the fringing field does not correspond to the measurement. Over the median plane the fringing field calculation extends the measurement, as can be expected for the 90° pole edge.

VII. NUTCRACKER -- THE COMPUTER CODE

This section of the paper may be considered as a computer user's manual for the computer code NUTCRACKER. It is intended to help the engineer or physicist use the computer to solve magnet problems. No experience in computer coding is necessary.

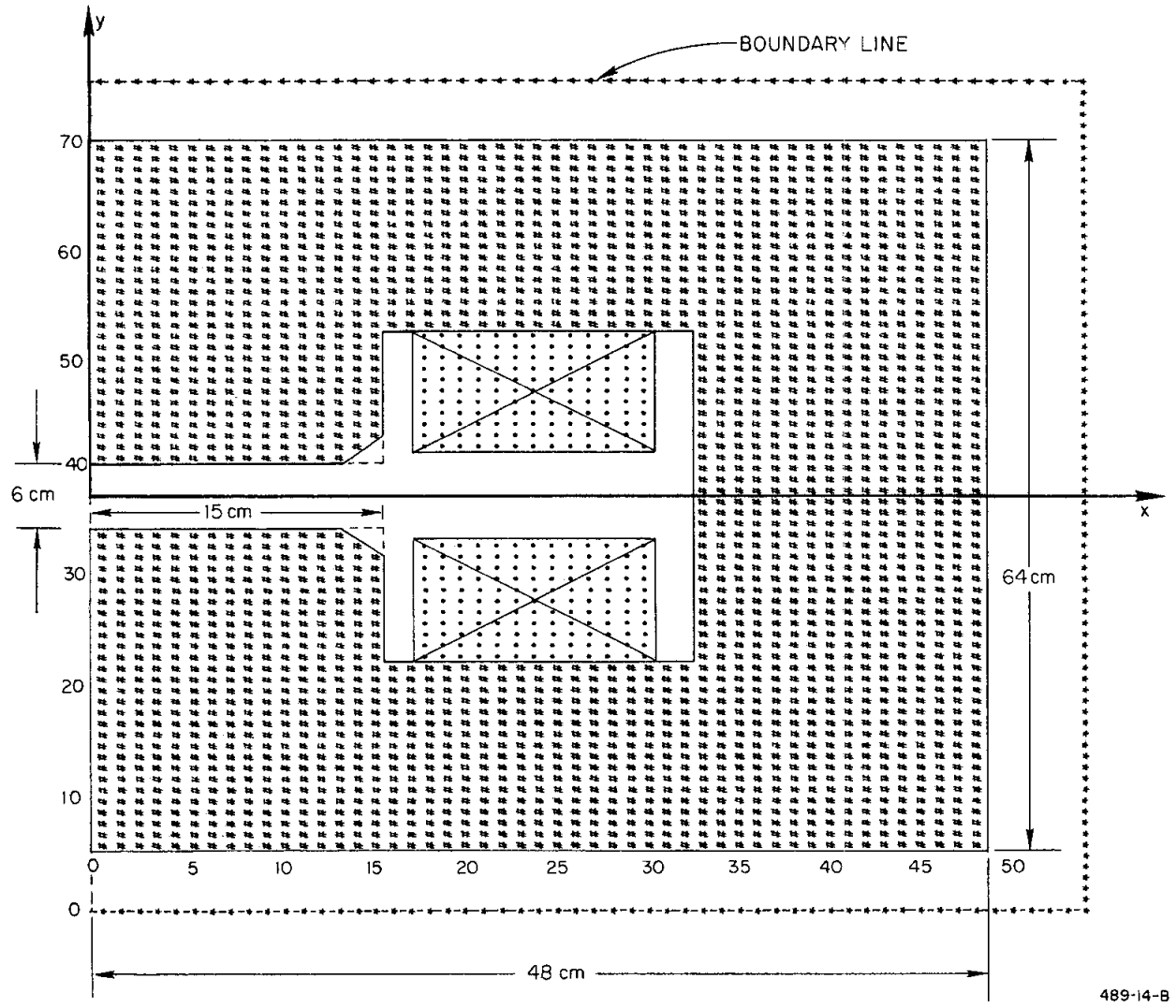

Fig. 11 - SLAC 3° BENDING MAGNET
EACH MARK IS THE CENTER
OF A 1 x 1 cm^2 MESH

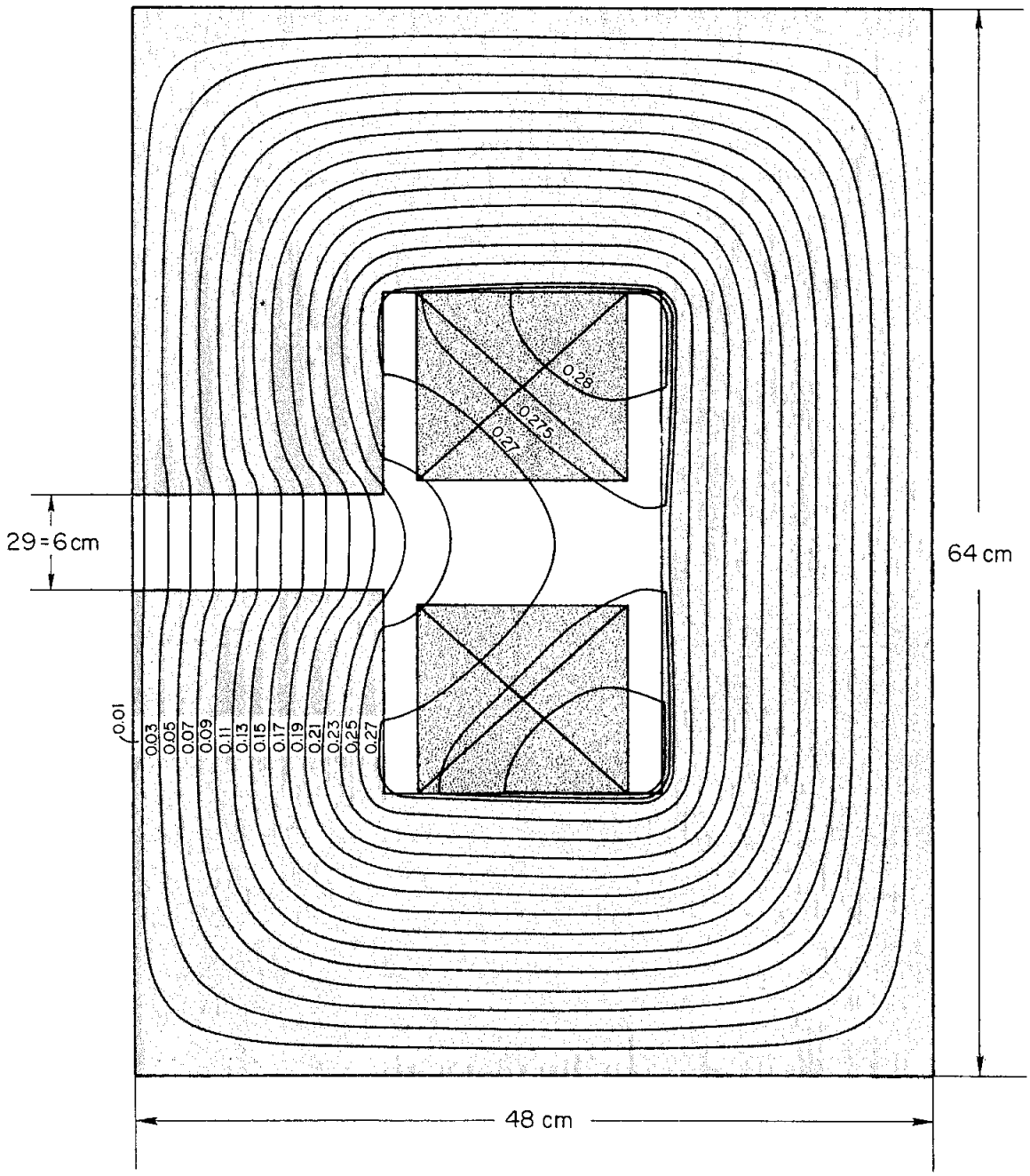

FIG. 12 -- SLAC 3° BENDING MAGNET. LINE OF CONSTANT VECTOR POTENTIAL

489-1-C

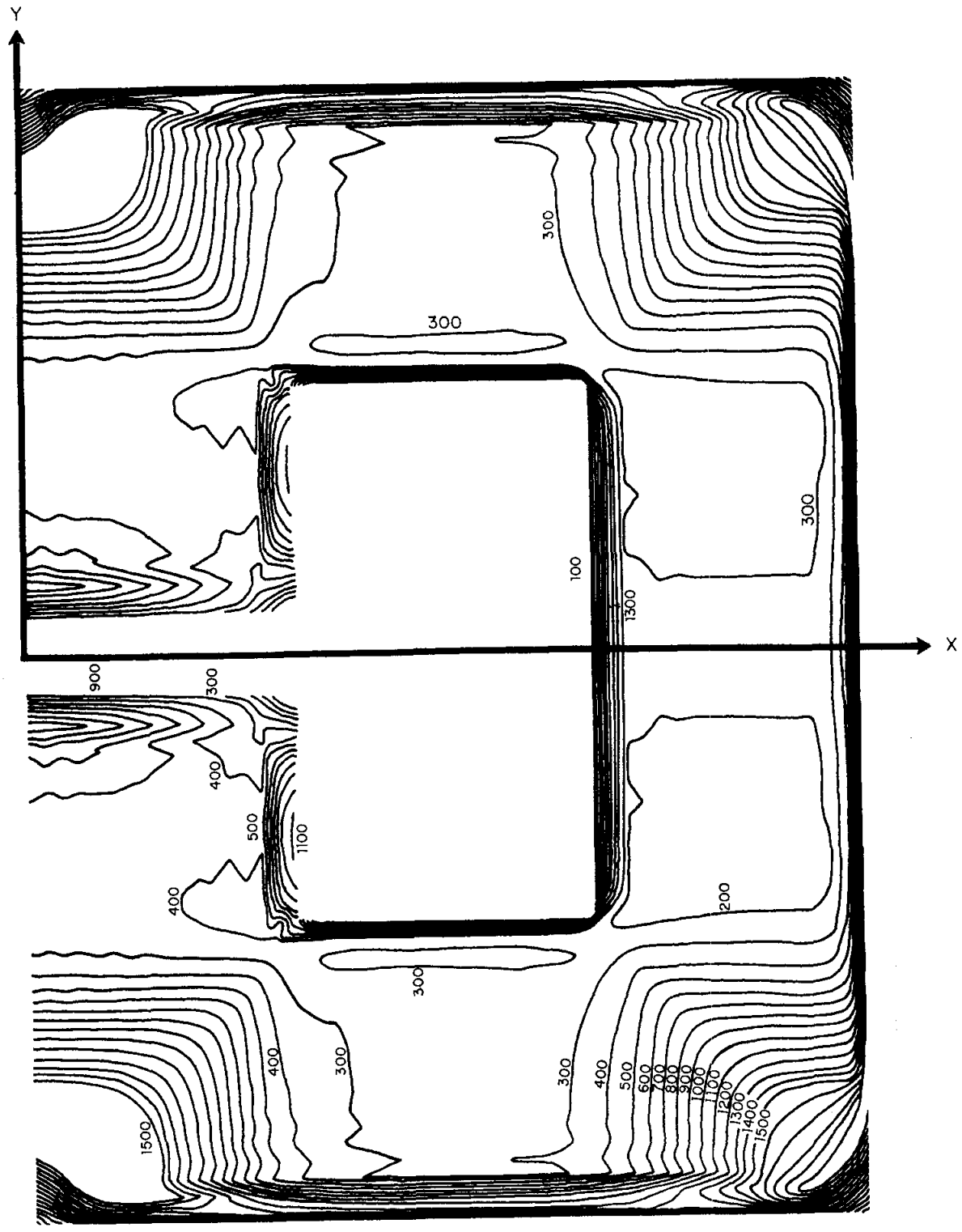

489-2-C

Fig. 13 – 3° BENDING MAGNET. LINE OF CONSTANT RELATIVE PERMEABILITY

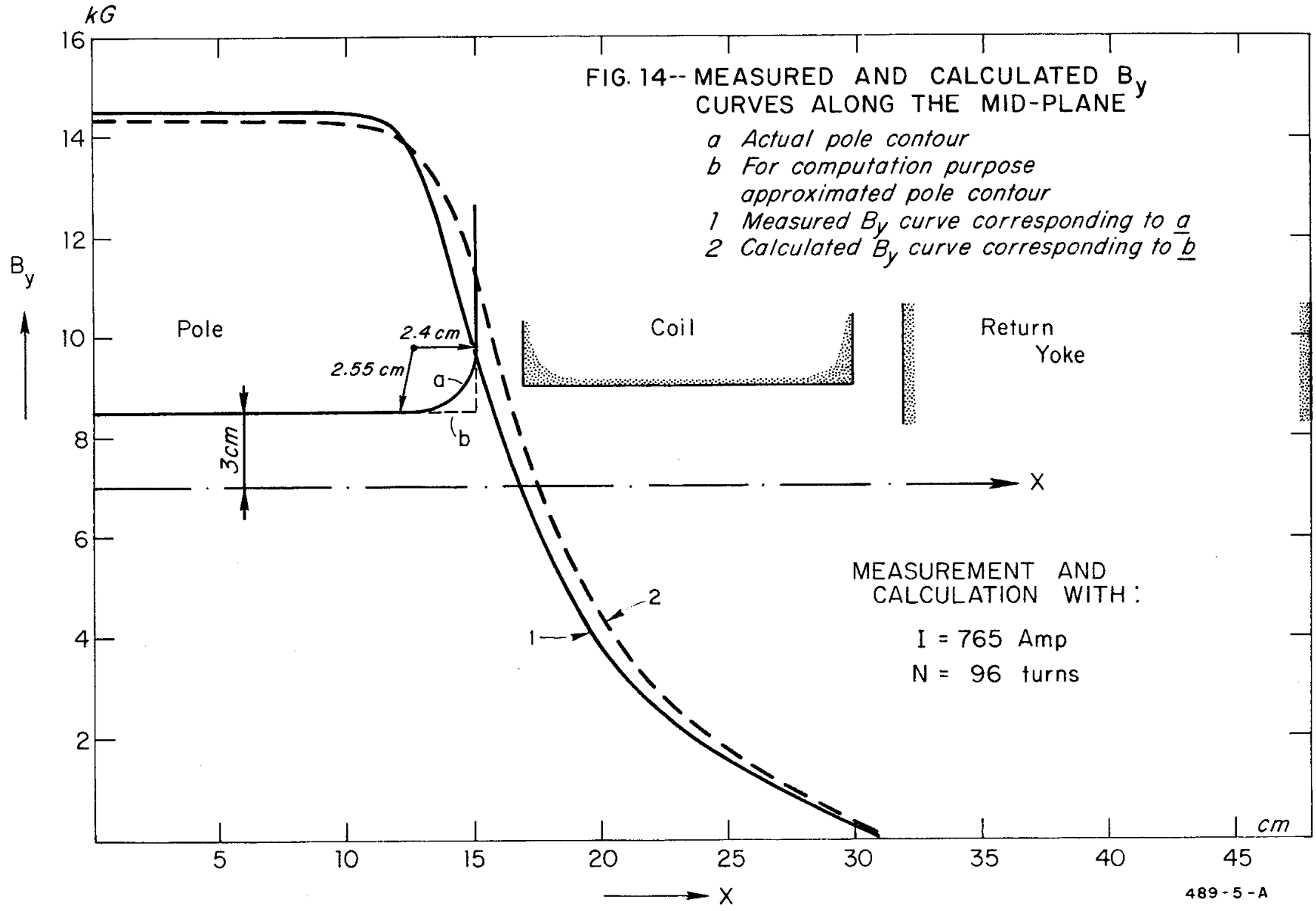

FIG. 14-- MEASURED AND CALCULATED B_y CURVES ALONG THE MID-PLANE

a Actual pole contour
b For computation purpose approximated pole contour
1 Measured B_y curve corresponding to a
2 Calculated B_y curve corresponding to b

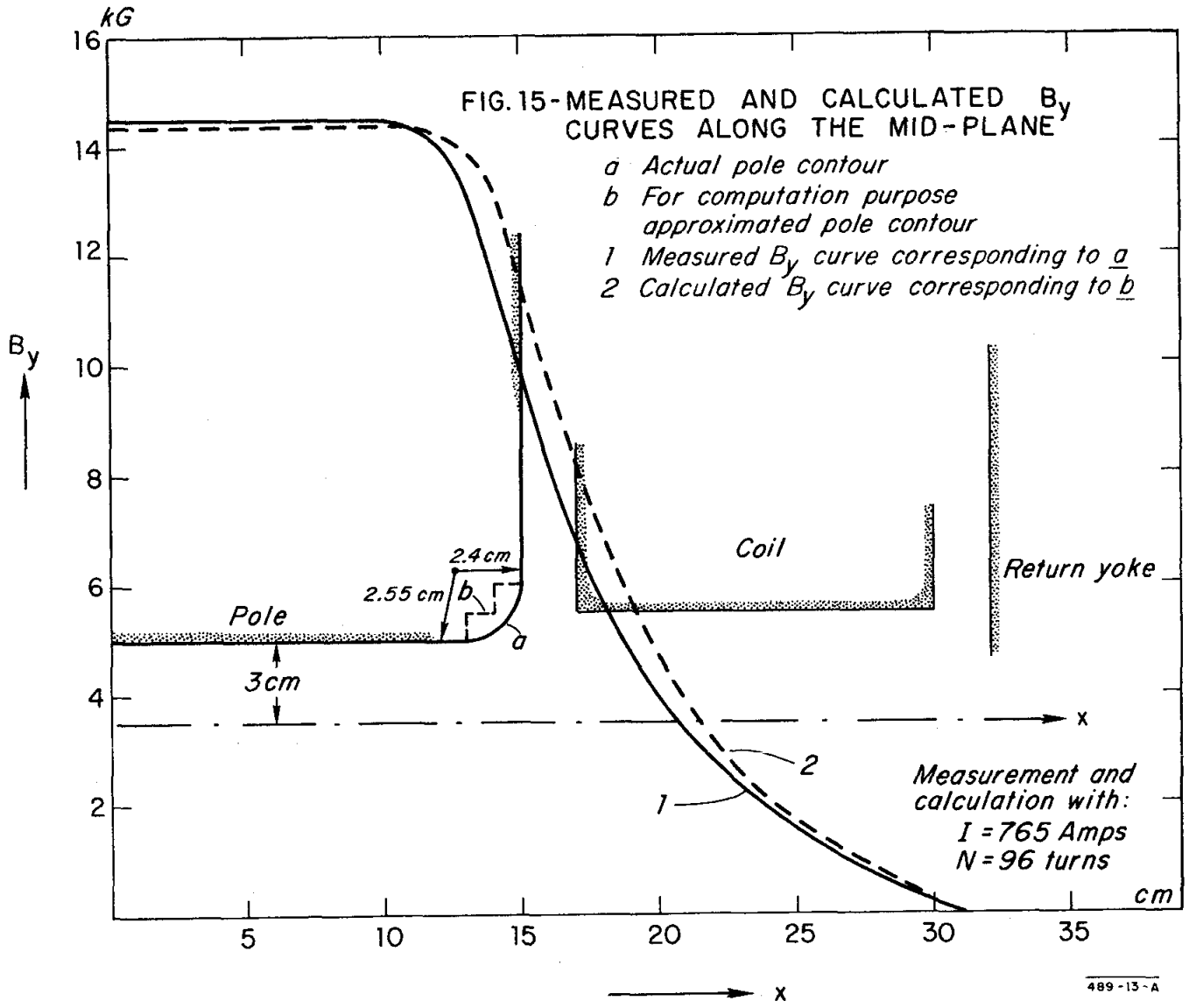
kG
16
14
12
10
8
6
4
2
B_y
FIG. 15 - MEASURED AND CALCULATED B_y CURVES ALONG THE MID-PLANE
a Actual pole contour
b For computation purpose approximated pole contour
1 Measured B_y curve corresponding to a
2 Calculated B_y curve corresponding to b
Coil
Return yoke
Pole
2.4 cm
2.55 cm
b
a
3 cm
x
2
1
Measurement and calculation with:
I = 765 Amps
N = 96 turns
cm
5
10
15
20
25
30
35
x
489-13-A

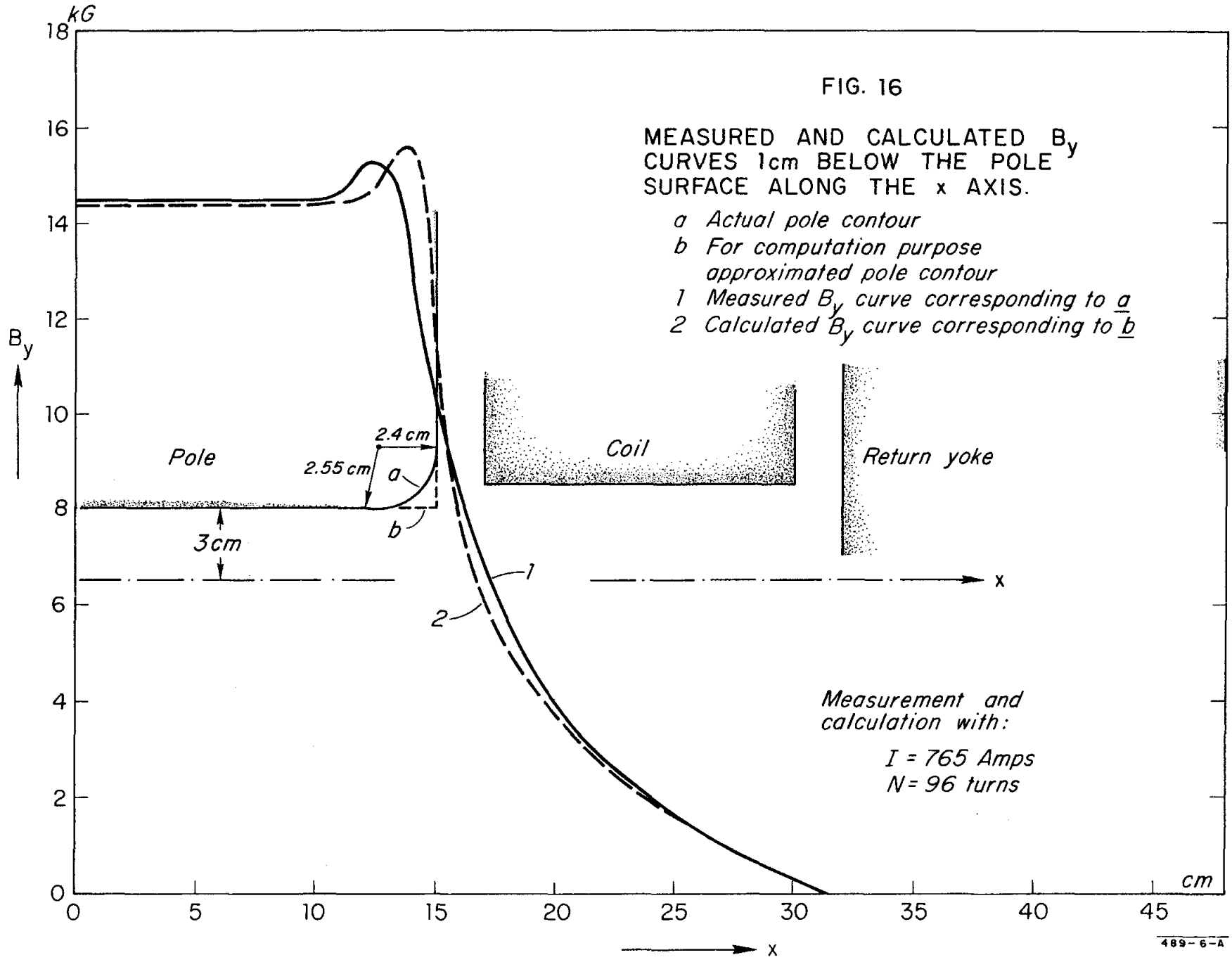

FIG. 16

MEASURED AND CALCULATED B_y CURVES 1cm BELOW THE POLE SURFACE ALONG THE x AXIS.

a Actual pole contour
b For computation purpose approximated pole contour
1 Measured B_y curve corresponding to a
2 Calculated B_y curve corresponding to b

NUTCRACKER was written in Extended ALGOL 60 for the Burroughs B5500 computer and runs in 16K of memory. The B5500's computing speed is comparable to one-third the IBM 7090 speed. All computing times mentioned in this report must be scaled by a factor of 3 to get a rough 7090 equivalent time.

Often in a program outline, important concepts are concealed in words, and not until a mistake is made are they uncovered. For this reason the necessary concepts are stated as rules to underline their importance.

All data are input in free-field format, i.e., relatively independent of position on the card. (For a more exact definition of Free Field Input see B5500 notes, Computation Center, Stanford University, California, Oct. 1964.)

Rule 1: All data are in free-field format.

In preparing a problem for NUTCRACKER one must first consider the mesh size and the number of nodes to be matched to the capacity of the computer. A square mesh was used to minimize computing time. The finite difference equations become more complicated as the mesh becomes more irregular.[12] Thus a mesh unit in the x or z direction must be the same as a mesh unit in the y or r direction. This can be obtained by the proper choice of the number of nodes in the x or z and y or r directions.

Rule 2: The mesh must be square.

The number of nodes must be limited due to memory limitations and the rate of convergence. A 50 × 60 mesh requires 6000 words of memory just to represent the vector potential and permeability. Due to properties of the B5500 (data descriptors), the 30 × 70 mesh problem (where the first number represents the number of nodes in the x or z direction and the second the y or r direction) runs faster than the 70 × 30 mesh problem.

With the choice of the size of the mesh unit completed, one must lay out the approximation on graph paper, with nodes at the intersection of graph lines.

The outer nodes represent boundary conditions ($\vec{A} = 0$). With the exception of these nodes, each node represents an h·h square in two-dimensional space. The air, iron, and coil boundaries lie between the nodes (see Fig.17).

Rule 3: The outer boundary is dislocated half a mesh unit from the boundary of the first square. (See Fig. 18.)

A rectangular block of iron or current-carrying conductor is specified by two sets of coordinates. The first is the coordinate of the lower left-hand node of the rectangle and the second, the upper right-hand node.

Rule 4: Blocks are specified by the lower left-hand and upper right-hand coordinates of a node.

When a block is a current-carrying conductor, the current is assumed to be uniformly distributed. Hence, current density is constant over the rectangle. $\vec{S}$ is positive out of the paper and negative into the paper. A fill factor should be included when specifying the current density. The z or θ direction is assumed.

Rule 5: Current density is positive outward, negative inward, and should include a fill factor.

The line integral $\oint \vec{H} d\vec{\ell}$ is used to increase the convergence rate and should be chosen with care. Magnet corners should be avoided, and when the path runs parallel to a magnet boundary there should be at least two nodes between the magnet boundary and the path.

The line integral is split into two components, and the path must run parallel to one of the axes. The reason for this is clear when the line integral over a path Γ is written as

$$\oint_{\Gamma} \vec{H} \cdot d\vec{\ell} = \int_{\Gamma} \vec{H}_x d\vec{x} + \int_{\Gamma} \vec{H}_y d\vec{y} \tag{73}$$

or in cylindrical coordinates

$$\oint_{\Gamma} \vec{H} \cdot d\vec{\ell} = \int_{\Gamma} \vec{H}_z d\vec{z} + \int_{\Gamma} \vec{H}_r d\vec{r} \quad . \tag{74}$$

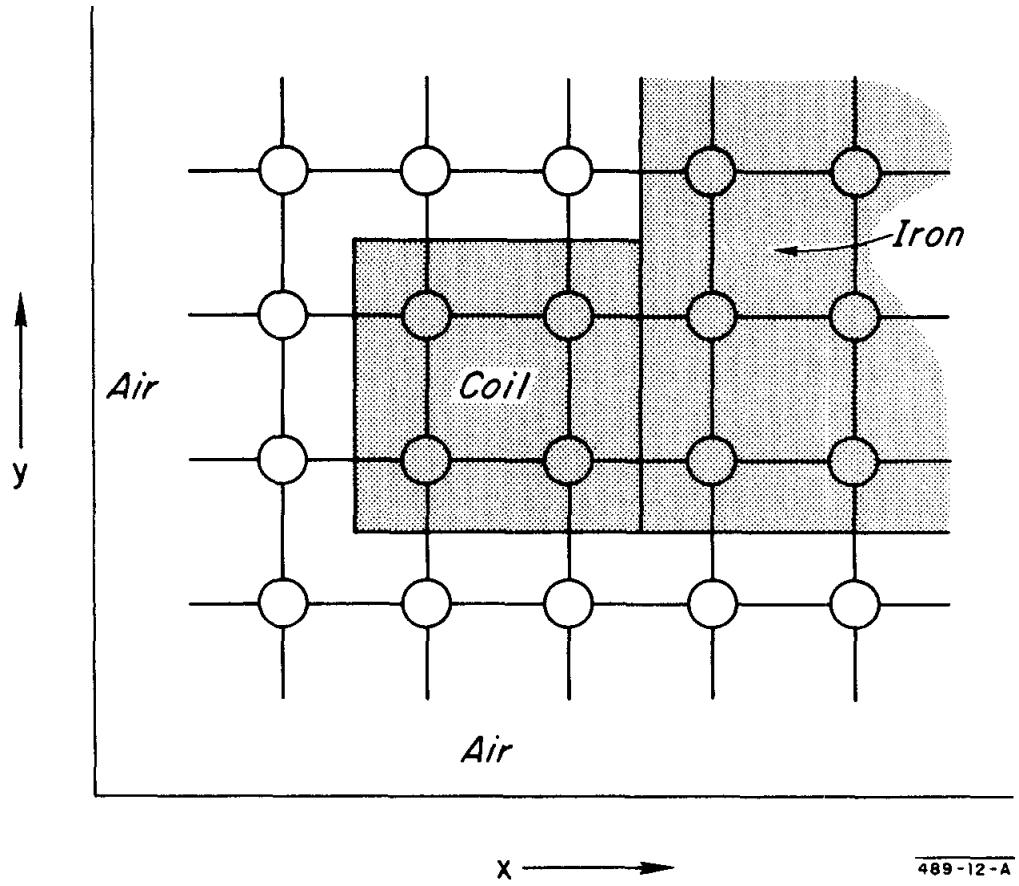

FIG. 17 -- MESH POINTS AND BOUNDARIES

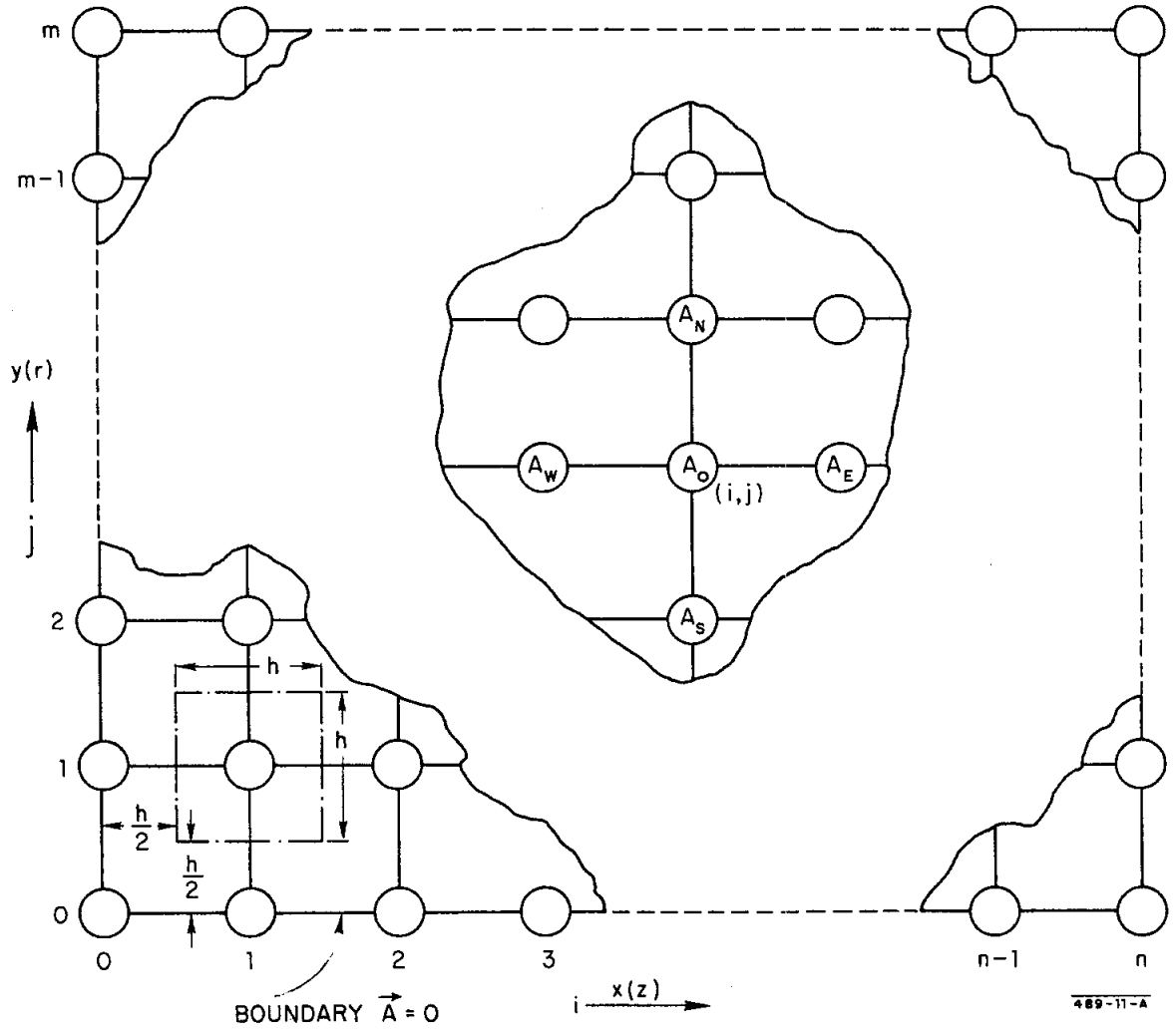

FIG. 18-- MESH ARRANGEMENT

The integration is done by the trapezoidal rule and each section of the path requires a minimum of three nodes. A minimum of four sections specified by five sets of coordinates are needed to define the closed positive path.

Rule 6: The closed line integral follows a counter-clockwise path specified by a minimum of five sets of coordinates (four sections) with each section parallel to one axis.

The calculation of the line integral is used to scale the vector potentials as mentioned earlier. The scaling factor C_m is calculated from the known ampere-turns in the system, IN, and the field intensity as follows:

$$C_m = \frac{\oint \vec{H} \cdot d\vec{\ell}}{IN} \quad . \tag{75}$$

Only the vector potentials in a rectangular region are scaled. This region is known as the area of influence and is specified by the lower left-hand and upper right-hand nodes of the rectangle. The path of the line integral must be within the area of influence and cannot lie on the boundary of the area of influence.

Rule 7: The path of the line integral is properly contained in the area of influence.

If the previous seven rules are followed, the errors in program setup will be minimized.

The data is input on cards and if necessary may be continued onto an extra card, but the data must start on a new card when specified. For a list of input parameters, associated identifiers and meaning, see Table I.

The order of data on cards is specified in Table II. As many cases as desired may be input.

The condition for the appearance of a data card or the repetition of a group of cards will be noted next to the cards with conditional appearance. The order of the items on a card must be preserved.

TABLE I

LIST OF INPUT PARAMETERS TO NUTCRACKER

Identifier	Physical Meaning or Operation Controlled	Value	Unit
CØØRDINATESYSTEM	coordinate system	0 rectangular 1 cylindrical	
XMESH	number of nodes on x axis	3 to 80	
YMESH	number of nodes on y axis	3 to 80	
ERRØR	tolerance on relaxation	1% = 0.01	
NIRØN	number of iron blocks	0 or greater	
NCØIL	number of coils	1 or greater	
ITERATIØNLIMIT	iteration limit	greater than 0	
PRINTREQUESTED	intermediate print requested	0,1*	
PHASE1REQUESTED	phase 1 requested	0,1*	
CØNTØURREQUESTED	contour plot of A requested	0,1*	
INITSØL	initial solution in air requested	0,1*	
NAME1	initial guess at μ and A requested	0,1*	
UNITIN	logical input unit	0,1,2,3,4**	
NAME2	output of μ and A requested	0,1*	
UNITØUT	logical output unit	0,1,2,3,4,5***	
X1	X coordinate	0 to 80	meters, mesh units
Y1	Y coordinate	0 to 80	meters, mesh units
X2	X coordinate	0 to 80	meters, mesh units
Y2	Y coordinate	0 to 80	meters, mesh units
CØNTØURMIN	minimum value of potential	any value C_{min}	
DELTACØNTØUR	difference between potential	any value $\Delta C \leq C_{max} - C_{min}$	
CØNTØURMAX	maximum value of potential	any value $C_{max} > C_{min}$	
NCURVES	number of curves	1 to 10	
NPØINTS	number of points in the curve	5 to 20	
J	current density	any value	amperes/meter^2

* 0 not requested, 1 requested

** 0 card reader
1, 2, 3, 4 tapes
tape 1 is released for output

*** 0 card punch
1, 2, 3, 4 tapes
5 line printer

TABLE II

DATA INPUT TO THE COMPUTER

Card Number	Condition	Data Items	Comments
1	always present	COORDINATESYSTEM, XMESH, YMESH, ERROR, NIRON, NCOIL, ITERATIONSLIMIT, PRINTREQUESTED, PHASEIREQUESTED, CONTOURREQUESTED, UNITSOL, NAME1, UNITIN, NAME2, UNITOUT, X1, Y1, X2, Y2.	X1 Y1 X2 Y2 specify the lower left-hand and upper right-hand coordinates of the total mesh in meters.
2	contour plot of $\vec{A}$ requested = 1.	CONTOURMIN, DELTACONTOUR, CONTOURMAX.	See Table I.
3	always present	NCURVES	See Table I.
4	repeat cards 4 and 5 NCURVES times (if card 4 used card 5 necessary)	NPOINTS X1 Y1 X2 Y2 .	X1, Y1, X2, Y2 specify area of influence in node coordinates
5		X1, Y1, S2, Y2, X3, Y3, ...XNPOINTS, YNPOINTS.	X1, Y1 etc. specify path of line integral in node coordinates
6	repeat NCOIL times	X1 Y1 X2 Y2 J	X1 Y1 X2 Y2 specify area of current carrying conductor in node coordinates
7	repeat NIRON times	X1 Y1 X2 Y2	X1 Y1 X2 Y2 specify area of iron block in node coordinates
8	cylindrical coordinates, repeat until X1=Y1=X2=Y2=0	X1 Y1 X2 Y2	X1 Y1 X2 Y2 specify area over which forces should be summed in node coordinates

PLANNED FURTHER ADDITIONS TO THE NUTCRACKER PROGRAM

1. The present code is slow. Computation time for large magnets takes several hours on the B5500. Rewriting the code in PL/I on a fast computer will speed up the process.
2. The NUTCRACKER program exclusively uses the solution of quasi-Poisson equations. In areas with constant permeability the use of Poisson[13] and even Laplace equations seems to be appropriate. The revised codification will comply with this requirement.
3. Appropriate use of Neuman and Cauchy boundary conditions where $\mu_r \gg 1$.
4. Different mesh distance and variable mesh size over the entire area to cut down computation time and improve resolution.
5. Solution for curved boundaries with variable μ_r values.

These improvements and the achieved results will be reported at a later date.

REFERENCES

1. F. Bitter, Rev. Sci. Instr. 7, 479-481 (1936).
2. D. B. Montgomery, "Some Useful Information for the Design of Iron Magnets," MIT, NML, (1962).
3. S. Schechter, "Iteration Methods for Nonlinear Problems." Trans. Amer. Math. Soc. 104, 179 (1962).
4. P. Concus, "On the Calculation of Nonlinear Magnetic Fields," Proc. Internat'l Symp. on Magnet Technology, Stanford Linear Accelerator Center, September 1965; pp. 164-169.
5. S. V. Ahamed, "Accelerated Convergences of Numerical Solution of Linear and Nonlinear Field Problems with Numerous Sources," Univ. Colorado Computor Journal, Boulder, Colorado (April 1965).
6. S. V. Ahamed, "Accelerated Convergence of Numerical Solution of Linear and Nonlinear Vector Field Problems," Univ. Colorado, Boulder, Colorado (1965).
7. S. R. Frankel, "Convergence Rates of Iterative Treatments of Partial Differential Equations," Math. Tables and Other Aids to Computation, 4, 65-75 (1950).
8. K. J. Binns and P. J. Larenson, Analysis and Computation of Electric and Magnetic Field Problems (McMillan Co., N.Y., 1963); pp. 251-297.
9. M. G. Salvadori and M. L. Baron, Numerical Methods in Engineering (Prentice Hall, Inc. Englewood Cliffs, N. J., 1959); p. 81.
10. H. Brechna, E. Burfine, R. Mizrahi and A. Wolff, "Two-Meter Spark Chamber Magnet Model," SLAC Report No. 57, Stanford Linear Accelerator Center, Stanford, California (1966).

11. B. Hedin, "A Bending Magnet with Nonsaturating Shimming," SLAC Report No. 19, Stanford Linear Accelerator Center, Stanford, California (1963).

12. A. M. Winslow, "Magnetic Field Calculations in an Irregular Triangular Mesh," Proc. Internat'l Symp. Magnet Techn., Stanford Linear Accelerator Center, September 1965; pp. 170-181.

13. W. B. Herrmannsfeldt, "Poisson Equation Solving Program," SLAC Report No. 51, Stanford Linear Accelerator Center, Stanford, California (1965).